

Supporting information

# **Synthesis of Two New Polyoxometalate-Based Organic Complexes from 2D to 3D Structures for Improving Supercapacitor Performance**

*Zhe Sun<sup>a</sup>, Xiaojing Yu<sup>\*a</sup>, Qingfang Zhen<sup>a</sup>, Tingting Yu<sup>b\*</sup>, Xinming Wang<sup>a</sup>, Guixin Yang<sup>a</sup>, Yongbin Song<sup>a</sup>, and7 Haijun Pang<sup>\*a</sup>*

## **Table of contents**

### **Section 1 Experimental Section**

- I. Chemicals and materials**
- II. Synthesis of imbta**
- III. Synthesis of pybta**
- IV. Photographs of 1 & 2**
- V. Characterization methods**
- VI. Electrochemical measurements**
- VII. Preparation of electrodes**

### **Section 2 Supplementary structural figures and characterization information**

- I. Structural Description**
- II. A Discussion on Why Immobilizing POMs into MOFs Can Alleviate the Solubility Issues of POMs**
- III. FT-IR, PXRD of 1 & 2**
- IV. Supercapacitor properties of 1- & 2-GCE**
- V. FT-IR of 1 immersed in a mixed solution of 0.5 M H<sub>2</sub>SO<sub>4</sub> + 0.5 M Na<sub>2</sub>SO<sub>4</sub> (v:v = 1:1) for 6, 12, 24, 48, and 96 h**
- VI. FT-IR of 2 immersed in a mixed solution of 0.5 M H<sub>2</sub>SO<sub>4</sub> + 0.5 M Na<sub>2</sub>SO<sub>4</sub> (v:v = 1:1) for 6, 12, 24, 48, and 96 h**
- VII. XRD of 1 and 2 immersed in a mixed solution of 0.5 M H<sub>2</sub>SO<sub>4</sub> + 0.5 M Na<sub>2</sub>SO<sub>4</sub> (v:v = 1:1) for 6, 12, 24, 48, and 96 h**

### **Section 3 References**

## Section 1 Experimental Section

### I. Chemicals and materials

All chemicals were purchased and used without further purification. Imidazole ( $C_3N_2H_4$ ,  $\geq 99.0\%$ , Beijing Ouhe Technology Co., Ltd.), benzotriazole ( $C_6N_3H_5$ ,  $\geq 99.0\%$ , Beijing Ouhe Technology Co., Ltd.), 18-C-6 ( $\geq 99.0\%$ , Beijing Ouhe Technology Co., Ltd.), 3-chloromethyl pyridine hydrochloride ( $C_6H_7ClN$ ,  $\geq 99.0\%$ , Beijing Ouhe Technology Co., Ltd.), phosphomolybdic acid ( $H_3[PMo_{12}O_{40}] \cdot 6H_2O$ ,  $PMo_{12}$ ),  $\geq 99.0\%$ , Shanghai Zhanyun Chemical CO., Ltd), silver nitrate ( $AgNO_3$ ,  $\geq 99.0\%$ , Shanghai Aladdin Biochemical Technology Co., Ltd.), sodium metavanadate ( $NaVO_3$ ,  $\geq 99.0\%$ , Shanghai Aladdin Biochemical Technology Co., Ltd.), triethyl amine ( $C_6H_{15}N$ ,  $\geq 99.0\%$ , Shanghai Aladdin Biochemical Technology Co., Ltd.), formaldehyde solution (HCHO, 36%, Shanghai Zhanyun), N, N-dimethylformamide ( $C_3H_7NO$ ,  $\geq 99.0\%$ , Shanghai Aladdin Biochemical Technology Co., Ltd.), dichlorosulfoxide ( $SOCl_2$ ,  $\geq 99.0\%$ , Shanghai Aladdin Biochemical Technology Co., Ltd.), sodium bicarbonate ( $NaHCO_3$ ,  $\geq 99.0\%$ , Shanghai Aladdin Biochemical Technology Co., Ltd.), Sodium chloride ( $NaCl$ ,  $\geq 99.0\%$ , Shanghai Aladdin Biochemical Technology Co., Ltd.), anhydrous sodium sulfate ( $NaSO_4$ ,  $\geq 99.0\%$ , Shanghai Aladdin Biochemical Technology Co., Ltd.), nitric acid ( $HNO_3$ , 1.0 M), sodium hydroxide ( $NaOH$ ,  $\geq 99.0\%$ , Shanghai Aladdin Biochemical Technology Co., Ltd.), Nafion (SIGMA), acetylene black (ACET, Shanghai Nuotai), PEG-600 (Tianjin Fuyu), anhydrous potassium carbonate ( $K_2CO_3$ ,  $\geq 99.0\%$ , Shanghai Aladdin Biochemical Technology Co., Ltd.), anhydrous acetonitrile ( $CH_3CN$ ,  $\geq 99.0\%$ , Shanghai Aladdin Biochemical Technology Co., Ltd.), ethyl acetate ( $CH_3COOC_2H_5$ ,  $\geq 99.0\%$ , Beijing Ouhe Technology Co., Ltd.), petroleum ether ( $\geq 99.0\%$ , Beijing Ouhe Technology Co., Ltd.).

## II. Synthesis of imbta.

The synthesis pathway for imbta<sup>1</sup> was established following the methodology outlined in, as depicted in Fig.S1. This synthetic process comprises three distinct steps, detailed as follows: The reaction mixture, comprising C<sub>6</sub>N<sub>3</sub>H<sub>5</sub> (bta, 6.8 g, 0.05 mol), formaldehyde solution (36%, 12 mL), and PEG-600 (2.5 mL), was heated under reflux for 1.5 h and subsequently cooled to room temperature. The resulting white precipitate was then filtered, washed, and dried. The resulting 1-hydroxymethylbenzotriazole (bmo) was used in the subsequent reaction without purification. Bmo was dissolved in 30 mL of N,N-dimethylformamide (DMF), 5 mL of SOCl<sub>2</sub> was added dropwise at room temperature, and the reaction mixture was stirred for 2 h. The pH was adjusted to 7 using a saturated NaHCO<sub>3</sub> solution, filtered, washed, and dried to obtain the crude product 1-chloromethylbenzotriazole (cbm). C<sub>3</sub>N<sub>2</sub>H<sub>4</sub> (1.6 g, 0.02 mol), K<sub>2</sub>CO<sub>3</sub> (3.3 g, 0.02 mol), and crown ether 18-C-6 (1.7 g, 6 mmol) were dissolved in 100 mL of anhydrous acetonitrile. After stirring for 0.5 h, cbm (3.4 g, 0.025 mol) was added to the reaction mixture, which was then heated under reflux for 2 h, concentrated, and extracted with ethyl acetate. The combined organic phases were washed with saturated brine, dried over anhydrous sodium sulfate, filtered, and concentrated under reduced pressure. The residue was purified by column chromatography and eluted with petroleum ether:ethyl acetate (2:1) to obtain imbition with a total yield of 62.5%. The structure of the product imbta was confirmed by <sup>1</sup>H-NMR spectroscopy, as shown in Fig.S2. The spectral data are as follows: <sup>1</sup>H-NMR (300 MHz, CDCl<sub>3</sub>) δ: 8.08 (d, 1H), 7.84 (s, 1H), 7.62-7.47 (m, 2H), 7.46-7.36 (m, 1H), 7.10 (d, 2H), 6.71 (s, 2H).

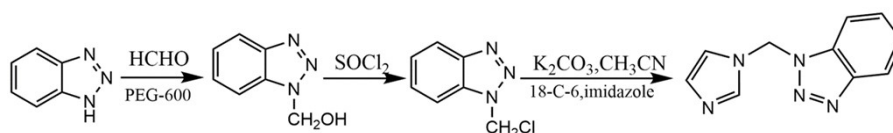


**Fig. S1.** The synthesis of imbta

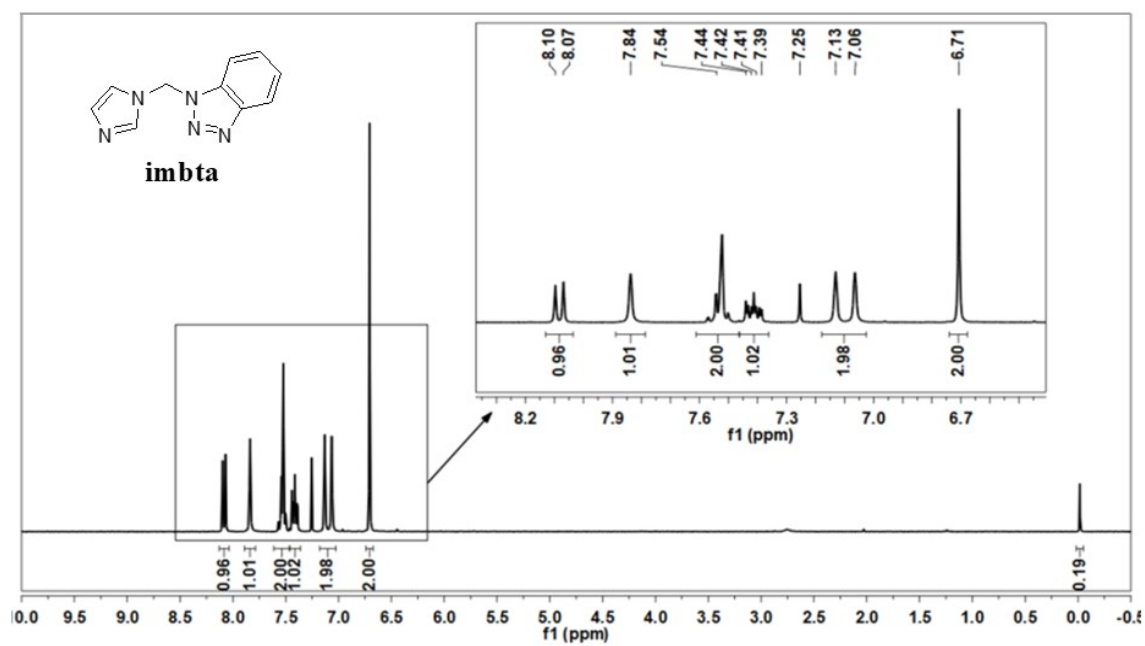


Fig. S2. The <sup>1</sup>H-NMR of imbta

### III. Synthesis of pybta.

The synthesis pathway for pybta<sup>2</sup> was established following the methodology outlined in a previous study. A synthetic pathway for pybta was developed, as depicted in Fig.S3. The detailed procedure is as follows: C<sub>6</sub>N<sub>3</sub>H<sub>5</sub> (bta) (4.84 g, 40 mmol), anhydrous potassium carbonate (8.28 g, 60 mmol), and 18-C-6 (0.52 g, 0.2 mmol) were individually added to a reaction flask containing 50 mL of anhydrous acetonitrile and stirred for 30 min. C<sub>6</sub>H<sub>7</sub>C<sub>12</sub>N (0.52 g, 0.2 mmol) was then added to the reaction flask and refluxed for 4 hours. The reaction progress was monitored using thin-layer chromatography (TLC). Upon completion, the reaction mixture was cooled to room temperature, filtered, and concentrated under reduced pressure. The crude product was recrystallized from a mixture of ethyl acetate and petroleum ether to yield a white needle-like solid in an approximate yield of 73.4%. The structure of pybta was confirmed by <sup>1</sup>H-NMR spectroscopy, as illustrated in Fig.S4. The data are as follows: <sup>1</sup>H-NMR (300 MHz, CDCl<sub>3</sub>) δ: 8.71 (s, 1H), 8.60 (d, 1H), 8.10 (d, 1H), 7.60 (d, 1H), 7.54-7.24 (m, 4H), 5.90 (s, 2H).

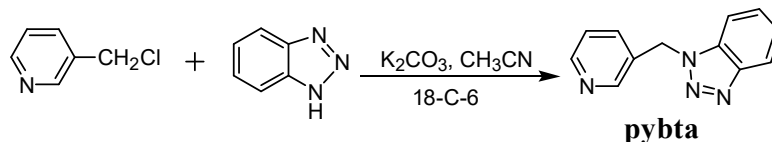


Fig. S3. The synthesis of pybta

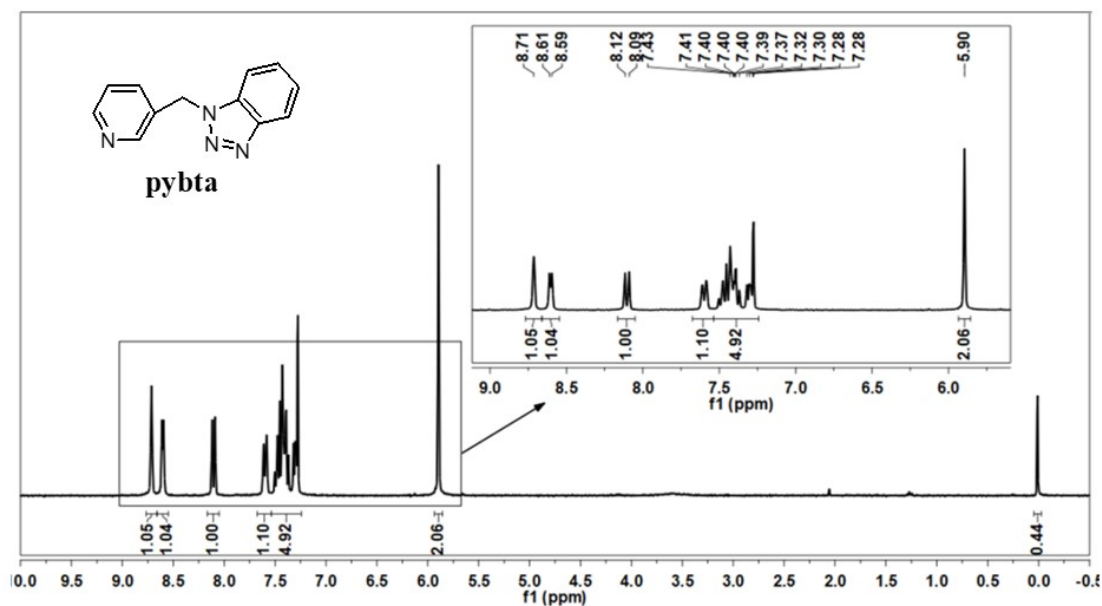
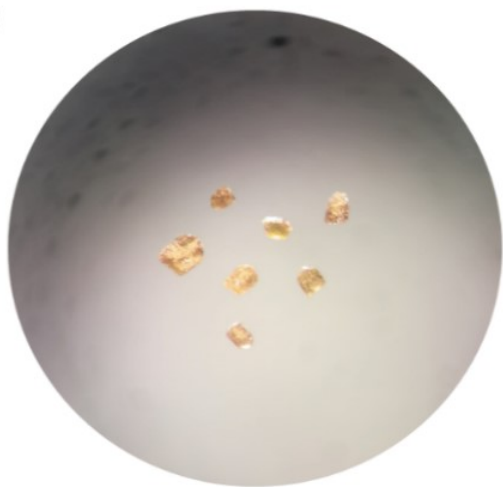


Fig. S4. The <sup>1</sup>H-NMR of pybta

#### IV. Photographs of 1 & 2

a)



b)

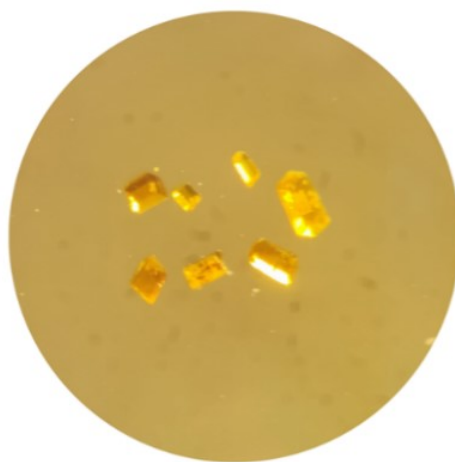


Fig. S5. The photos of a) 1, b) 2

## V. Characterization methods

Fourier-transform infrared spectroscopy (FT-IR) of **1** and **2** was conducted using an infrared spectrometer (Thorlabs, USA) in the wavenumber range of 400-4000  $\text{cm}^{-1}$ . Powder X-ray diffraction (PXRD) patterns were recorded on a Rigaku diffractometer (Nikaku, Japan) with Cu  $K\alpha$  radiation over a scanning range of 5–50°. X-ray photoelectron spectroscopy (XPS) was conducted using a K-Alpha instrument (Thermo Fisher Scientific, USA) with Al  $K\alpha$  radiation ( $h\nu = 1486.8$  eV) and charge correction at  $C_{1s} = 284.8$  eV. Single-crystal X-ray diffraction data for **1** and **2** were collected using a Bruker SMART CCD diffractometer at 296 K with graphite-monochromated Mo  $K\alpha$  radiation ( $\lambda = 0.71073$  Å). The structures were solved using the SHELXTL-2014 program with the direct method on  $F^2$  and refined using full-matrix least-squares on  $F^2$ . Non-hydrogen atoms were refined with anisotropic thermal parameters, whereas hydrogen atoms on the carbon atoms of the organic ligands imbta and pybta in **1** and **2** were included in the calculated positions.

## VI. Electrochemical measurements

The electrochemical workstation (CHI 760E) utilizes a three-electrode configuration to conduct electrochemical measurements in an electrolyte composed of 0.5 M H<sub>2</sub>SO<sub>4</sub> and 0.5 M Na<sub>2</sub>SO<sub>4</sub> (v:v=1:1). In this setup, the Ag/AgCl electrode served as the reference electrode, a Pt sheet functioned as the counter electrode, and a glassy carbon electrode (GCE) acts as the working electrode. Cyclic voltammetry (CV), constant current charge-discharge (GCD), and electrochemical impedance spectroscopy (EIS, 0.005–1000 kHz, loop potential) were employed to analyze the electrochemical performance. The specific capacitance of the working electrode was calculated based on the charge-discharge curves under varying current densities<sup>[3]</sup>.

**Method for obtaining the specific capacitance.** The specific capacitance of the working electrode was calculated based on the charge-discharge curves at various current densities<sup>[3]</sup>. The calculation formula (Equation S1) is as follows:

$$C_s = \frac{I\Delta t}{m\Delta V} \quad (S1)$$

Where  $C_s$  (F g<sup>-1</sup>) is the specific capacitance,  $I$  (A) is the discharge current,  $\Delta t$  (s) is the discharge duration,  $m$  (g) is the mass of the active electrode material, and  $\Delta V$  (V) is the potential window. Generally, the specific capacitance calculated from the galvanostatic charge-discharge (GCD) curve is considered more representative of the actual device performance than that obtained from Cyclic Voltammetry (CV) measurements.

The ion diffusion coefficient<sup>[4]</sup> ( $D$ ) for the working electrode was calculated based on the Warburg impedance derived from the EIS data. The  $D$  was calculated using the following equation:

The Warburg impedance ( $Z_\omega$ ) is related to ion diffusion in the electrolyte and can be expressed as:

$$Z_\omega = \delta\omega^{-1/2}(1-j) \quad (S2)$$

where  $\delta$  is the Warburg coefficient,  $\omega$  is the angular frequency,  $j$  is the imaginary unit.

The Warburg coefficient ( $\delta$ ) is calculated using the following relationship:

$$\delta = \frac{RT}{\sqrt{2}n^2F^2ACD^{1/2}} \quad (S3)$$

Rearranging the  $\delta$  equation to solve for  $D$ :

$$D = \frac{R^2 T^2}{2A^2 n^2 F^4 C^2 \delta^2} \quad (S4)$$

Where R is the gas constant (8.314 J mol<sup>-1</sup>·K<sup>-1</sup>), T is the temperature (298 K), A is the electrode area (1 cm<sup>2</sup> in this study), n is the number of electrons transferred (assumed to be 1 for simplicity), F is the Faraday constant (96485 C·mol<sup>-1</sup>) and C is the concentration of ions (0.5 mol·L<sup>-1</sup> for H<sub>2</sub>SO<sub>4</sub> + Na<sub>2</sub>SO<sub>4</sub>).

## **VII. The preparation method of the working electrode.**

Initially, the GCE was sequentially polished using  $\text{Al}_2\text{O}_3$  powder with particle sizes of 1  $\mu\text{m}$ , 0.3  $\mu\text{m}$ , and 0.05  $\mu\text{m}$  sequentially on a chamois surface, washed with water, and dried for subsequent use. Subsequently, the crystalline material and  $\text{PMo}_{12}$  were mixed with acetylene black at a mass ratio of 1:1 and the electrode material was prepared by grinding in an agate mortar for 2 h. The electrode material (6 mg) was dispersed in 300  $\mu\text{L}$  of deionized water and sonicated for 45 min to form a uniformly mixed slurry. Ten microliters of this slurry was deposited on the surface of the GCE and dried at room temperature for two days. Finally, the surface of the GCE was coated with 5  $\mu\text{L}$  of Nafion solution and dried for 12 h to prepare **1-GCE** and **2-GCE** modified with **1** and **2** and the working electrode  $\text{PMo}_{12}$ .

## **Section 2 Supplementary structural figures and characterization information**

## I. Structural Description

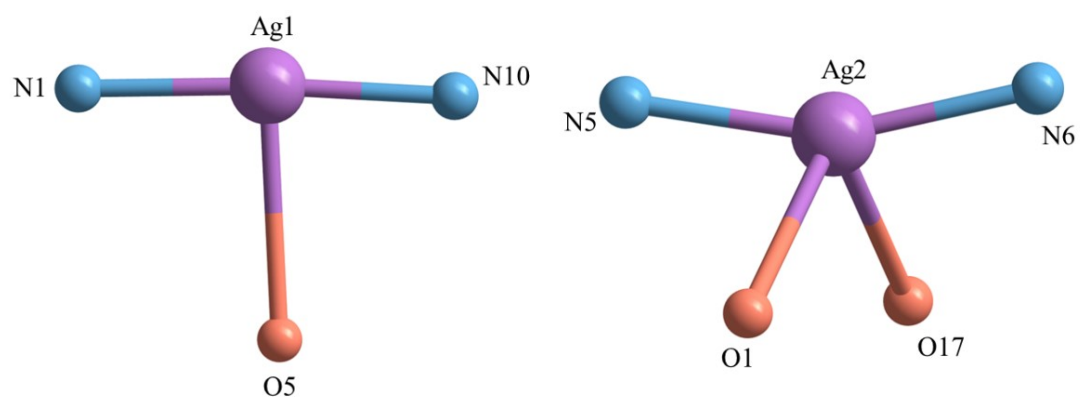


**Fig. S6.** The coordination patterns of Ag1 and Ag2

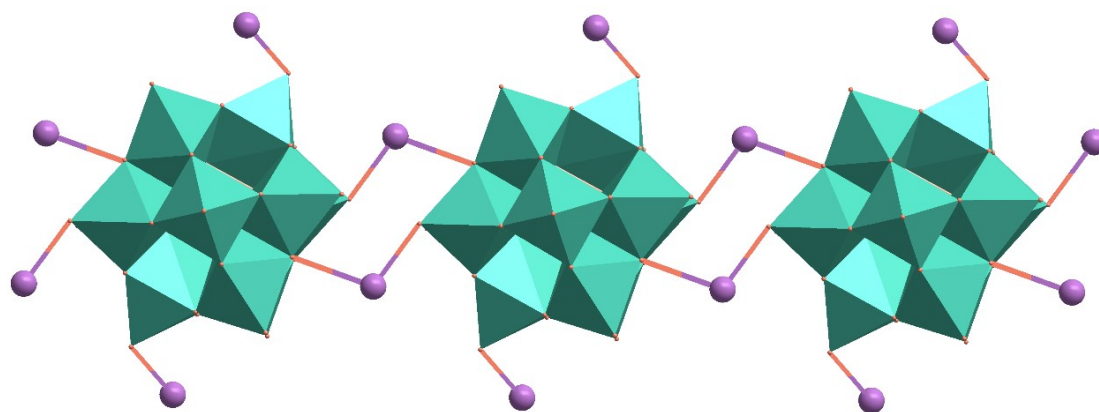


**Fig. S7.** The linear coordination structure of PMO<sub>12</sub> and Ag in **1**

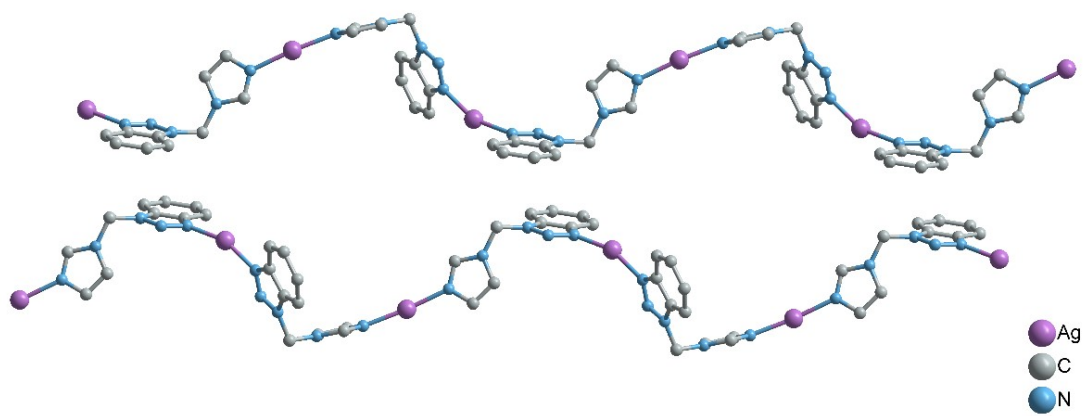


**Fig. S8.** The 1D chains formed by the coordination of imbta with Ag1 and Ag2

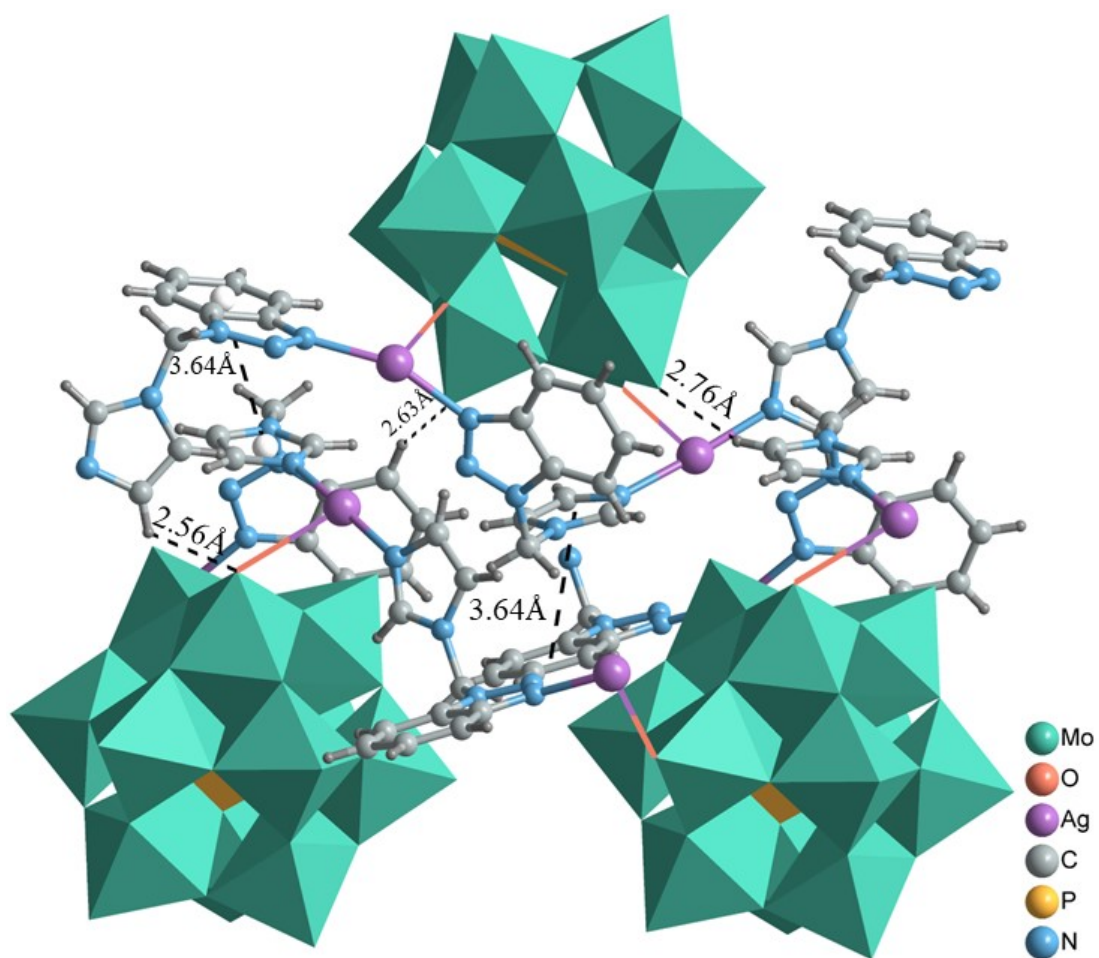


**Fig. S9.** The hydrogen bonding and  $\pi \cdots \pi$  interaction between adjacent 2D layers

**Table S1.** The selected bonds lengths (Å) and angles (°) for **1**

Mo(1)-O(15)	1.649(6)	Ag(2)-N(3)	2.134(7)	Mo(4)-O(21)	2.460(9)
Mo(1)-O(13)	1.857(7)	Ag(2)-N(4)	2.150(7)	Mo(4)-O(22)	2.471(10)
Mo(1)-O(4)	1.876(6)	C(1)-N(6)	1.376(11)	Mo(5)-O(10)	1.652(6)
Mo(1)-O(6)	1.908(6)	C(1)-C(3)	1.381(12)	Mo(5)-O(1)	1.859(7)
Mo(1)-O(5)	1.960(7)	C(2)-C(4)	1.388(12)	Mo(5)-O(11)	1.874(7)
Mo(1)-O(19)	2.416(10)	C(4)-N(4)	1.370(10)	Mo(5)-O(2)	1.922(6)
Mo(1)-O(21)	2.460(9)	C(5)-N(7)	1.329(12)	Mo(5)-O(22)	2.474(9)
Mo(2)-O(8)	1.643(6)	C(5)-N(2)	1.321(11)	Mo(6)-O(17)	1.656(6)
Mo(2)-O(7)	1.853(7)	Mo(3)-O(9)	1.645(6)	Mo(6)-O(11)	1.902(7)
Mo(2)-O(14)	1.873(7)	Mo(3)-O(18)	1.855(8)	Mo(6)-O(14)	1.923(7)
Mo(2)-O(4)	1.903(6)	Mo(3)-O(2)	1.885(7)	O(20)-O(22)	1.820(13)
Mo(2)-O(18)#1	1.960(8)	Mo(3)-O(12)	1.900(7)	O(22)-P(1)	1.492(9)
Mo(2)-O(20)#1	2.433(10)	Mo(3)-O(3)	1.946(7)	C(6)-C(13)	1.357(13)
O(19)-P(1)	1.543(10)	Mo(3)-O(20)	2.424(9)	C(6)-N(2)	1.366(11)
O(19)-O(21)	1.735(14)	Mo(4)-O(16)	1.649(6)	C(7)-N(1)	1.365(12)
O(20)-P(1)	1.597(9)	Mo(4)-O(5)	1.849(7)	C(19)-C(20)	1.318(16)
O(21)-P(1)	1.511(9)	Mo(4)-O(3)	1.860(6)	C(17)-C(19)	1.392(19)
Ag(1)-N(2)	2.110(7)	Mo(4)-O(1)	1.926(6)	C(17)-C(18)	1.408(18)
Ag(1)-N(1)#2	2.131(7)	Mo(4)-O(7)	1.961(6)	C(15)-N(9)	1.366(12)
O(15)-Mo(1)-O(13)	102.7(4)	Mo(5)-O(1)-Mo(4)	139.2(5)		
O(15)-Mo(1)-O(4)	103.0(4)	P(1)-O(19)-O(22)#1	54.2(4)		
O(13)-Mo(1)-O(4)	90.5(3)	P(1)-O(19)-Mo(1)	125.0(6)		
O(15)-Mo(1)-O(6)	100.4(4)	Mo(6)#1-O(20)-Mo(3)	93.8(3)		
O(13)-Mo(1)-O(6)	88.5(3)	N(2)-Ag(1)-N(1)#2	174.3(3)		
O(4)-Mo(1)-O(6)	156.2(4)	N(3)-Ag(2)-N(4)	158.7(3)		
O(15)-Mo(1)-O(5)	98.8(3)	N(6)-C(1)-C(3)	134.2(8)		
O(13)-Mo(1)-O(5)	158.3(4)	C(3)-C(1)-C(4)	122.0(9)		
O(4)-Mo(1)-O(5)	87.6(3)	C(16)-N(1)-Ag(1)#3	127.4(7)		
O(13)-Mo(1)-O(19)	64.4(4)	N(8)-N(3)-Ag(2)	119.4(6)		

---

Symmetry transformations used to generate equivalent atoms:

#1 -x+2, -y, -z; #2 x+1, y-1, z; #3 x-1, y+1, z

---

**Table S2.** The selected bonds lengths (Å) and angles (°) for **2**

P(1)-O(20)	1.493(9)	N(4)-Ag(2)	2.190(8)	O(20)-Mo(5)	2.455(9)
P(1)-O(18)	1.505(10)	O(4)-Mo(4)	1.881(6)	O(20)-Mo(4)	2.428(9)
P(1)-O(19)	1.535(9)	O(4)-Mo(1)	1.909(7)	C(20)-C(24)	1.383(13)
P(1)-O(14)	1.598(10)	N(5)-Ag(1)#2	2.142(8)	O(19)-Mo(3)	2.446(10)
O(1)-Mo(2)	1.859(7)	O(5)-Mo(7)	1.650(6)	O(19)-Mo(5)	2.412(9)
O(1)-Mo(3)	1.935(7)	C(6)-C(16)	1.360(17)	O(18)-Mo(6)	2.465(9)
C(1)-C(7)	1.373(14)	O(6)-Mo(5)	1.855(6)	O(18)-Mo(3)	2.474(9)
C(1)-C(21)	1.398(12)	O(6)-Mo(7)	1.924(7)	C(19)-C(21)	1.383(12)
N(1)-N(5)	1.309(11)	N(7)-Ag(1)	2.149(8)	O(18)-O(19)	1.753(13)
N(1)-N(3)	1.347(11)	O(7)-Mo(3)	1.671(6)	O(17)-Mo(6)	1.906(6)
C(2)-N(4)	1.334(13)	O(8)-Mo(3)	1.891(7)	O(17)-Mo(2)	1.896(6)
C(2)-C(7)	1.366(14)	O(8)-Mo(5)	1.902(6)	O(16)-Mo(7)	1.856(8)
N(2)-Ag(2)	2.186(8)	O(23)-Mo(5)	1.905(6)	O(15)-Mo(6)	1.646(9)
O(2)-Mo(3)	1.893(7)	O(23)-Mo(1)	1.865(7)	O(14)-Mo(7)	2.444(9)
O(2)-Mo(6)	1.900(6)	C(23)-C(24)	1.350(14)	C(14)-C(17)	1.492(14)
C(3)-C(11)	1.375(13)	O(22)-Mo(2)	1.894(7)	O(13)-Mo(1)	1.650(6)
C(3)-C(6)	1.396(14)	O(22)-Mo(1)	1.893(8)	O(12)-Mo(5)	1.888(6)
O(3)-Mo(3)	1.880(7)	C(22)-C(23)	1.419(14)	O(12)-Mo(4)	1.900(7)
O(3)-Mo(7)	1.931(7)	O(21)-Mo(7)	1.864(7)	O(11)-Mo(2)	1.657(6)
O(20)-P(1)-O(18)	112.0(5)	C(2)-N(4)-Ag(2)	121.3(6)		
O(20)-P(1)-O(19)	66.9(5)	O(13)-Mo(1)-O(23)	101.8(3)		
O(20)-P(1)-O(14)	108.0(5)	O(13)-Mo(1)-O(22)	101.8(4)		
O(18)-P(1)-O(14)	107.5(5)	O(23)-Mo(1)-O(4)	88.1(3)		
O(19)-P(1)-O(14)	73.6(5)	O(22)-Mo(1)-O(4)	157.4(4)		
Mo(2)-O(1)-Mo(3)	138.8(4)	O(13)-Mo(1)-O(4)	100.5(3)		
C(7)-C(1)-C(21)	119.3(9)	O(23)-Mo(1)-O(22)	90.6(3)		
N(5)-N(1)-N(3)	107.4(8)	P(1)-O(20)-O(19)	57.7(5)		
N(4)-C(2)-C(7)	124.2(9)	P(1)-O(20)-Mo(5)	126.3(5)		
N(6)-N(2)-Ag(2)	116.1(6)	C(19)-C(21)-C(1)	5-22.2(8)		

---

Symmetry transformations used to generate equivalent atoms:

#1  $-x+1, y, -z+1/2$ ; #2  $-x+3/2, y-1/2, -z+1/2$ ; #3  $-x+3/2, y+1/2, -z+1/2$

---

## **II. A Discussion on Why Immobilizing POMs into MOFs Can Alleviate the Solubility Issues of POMs:**

In general, the POMs possess many surface oxygen atoms with high negative charges and the metal atoms in MOF possess unoccupied orbital, and thus POMs and MOFs are easily coordinated together to form POMOFs, which alleviates the solubility of POMs.

Additionally, in this work, the Keggin-type POMs have been successfully encapsulated into metal-organic frameworks (MOFs) under a hydrothermal method. And it is a common phenomenon that such POMOFs obtained by hydrothermal method generally have poor solubility.<sup>[5]</sup> Thus, the title POMOFs structure can alleviate the solubility of POMs in water.

### III. FT-IR, PXRD of 1 & 2

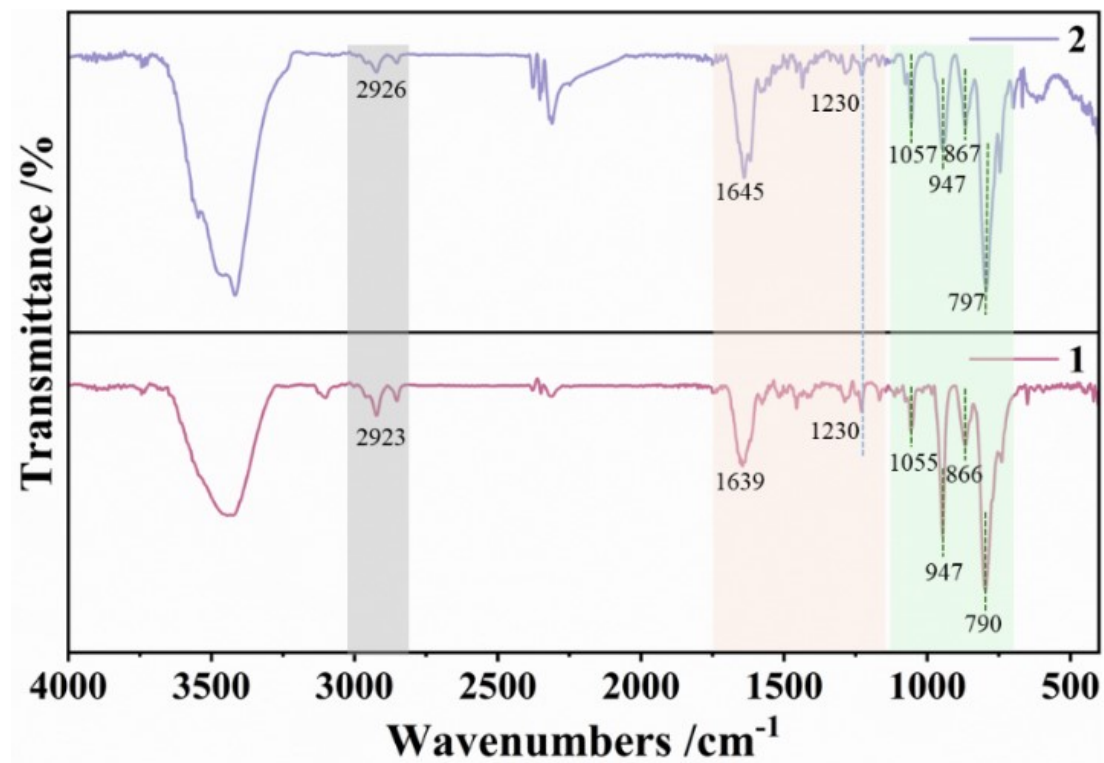
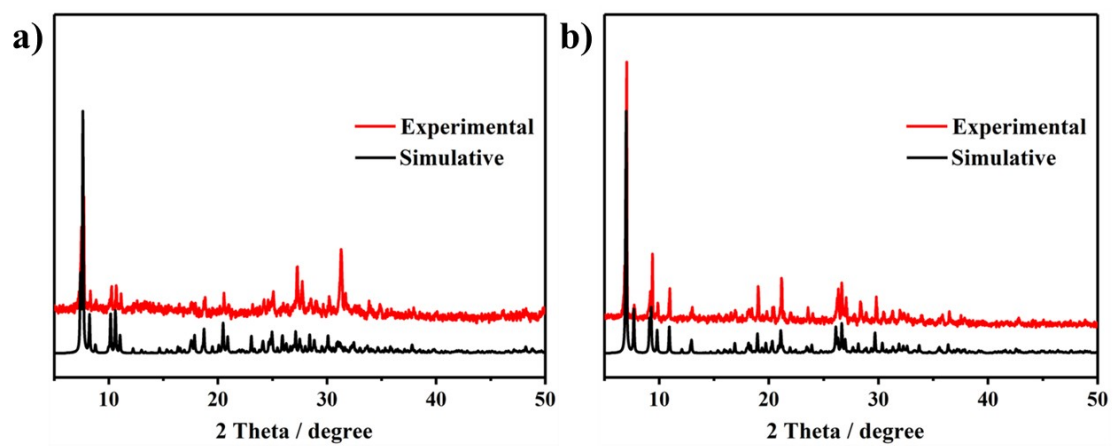


Fig. S10. The FT-IR of 1 and 2



**Fig. S11.** The XRD of a) 1 and b) 2

#### IV. Supercapacitor properties of 1- & 2-GCE

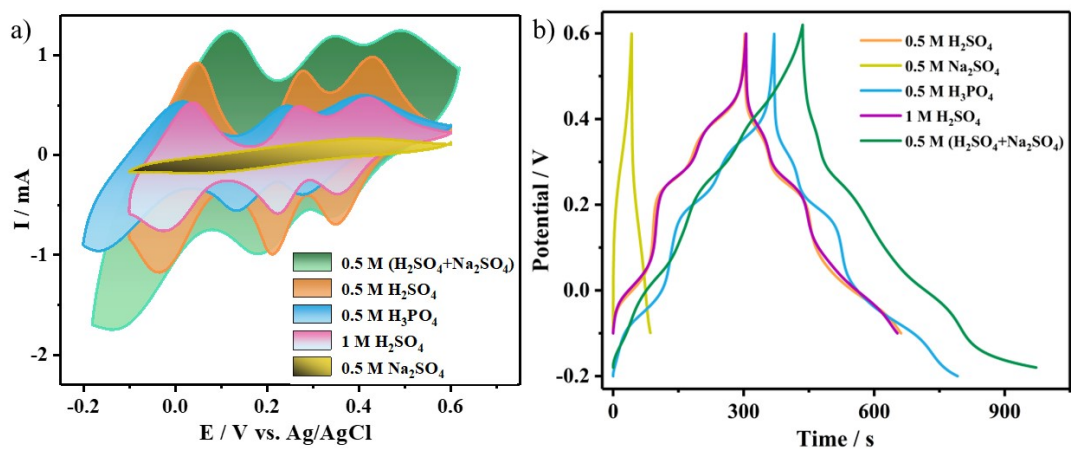
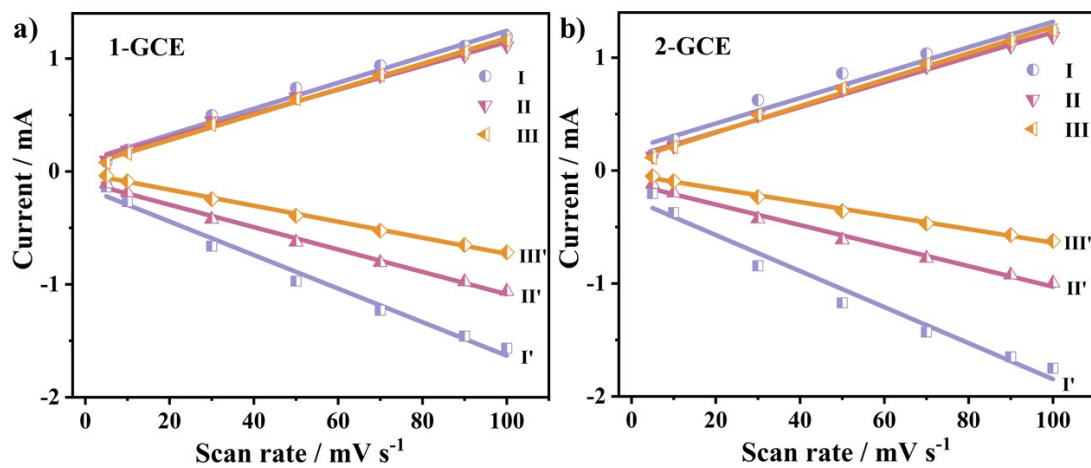
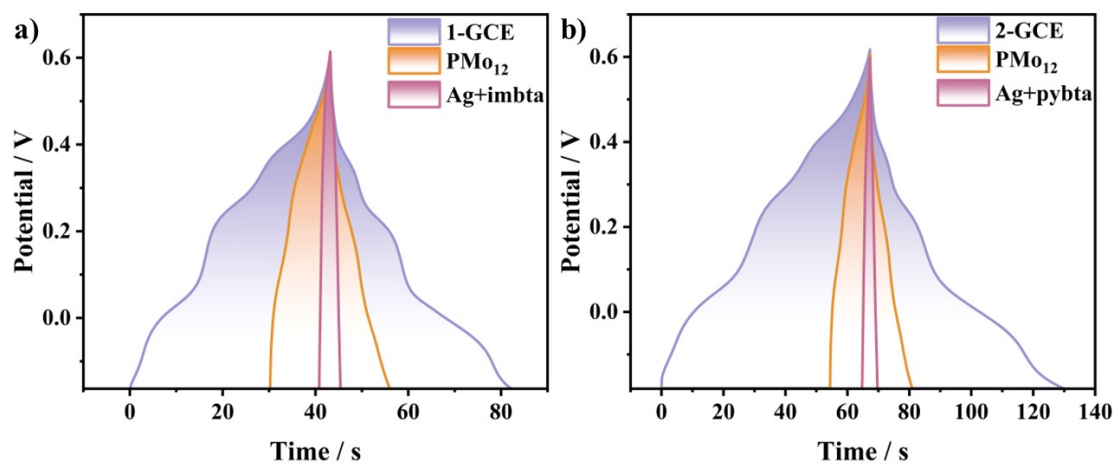


Fig. S12. 2-GCE in different electrolyte solutions: a) the CV at  $100 \text{ mV} \cdot \text{s}^{-1}$ , b) the GCD at  $1 \text{ A} \cdot \text{g}^{-1}$



**Fig. S13.** The linear relationship between the three pairs of redox peak currents and sweep velocities for a) 1-GCE and b) 2-GCE.



**Fig. S14.** a) 1-GCE, PMo<sub>12</sub>, and imbta + AgNO<sub>3</sub>; b) 2-GCE, PMo<sub>12</sub>, and pybta + AgNO<sub>3</sub> at 5 A g<sup>-1</sup>.

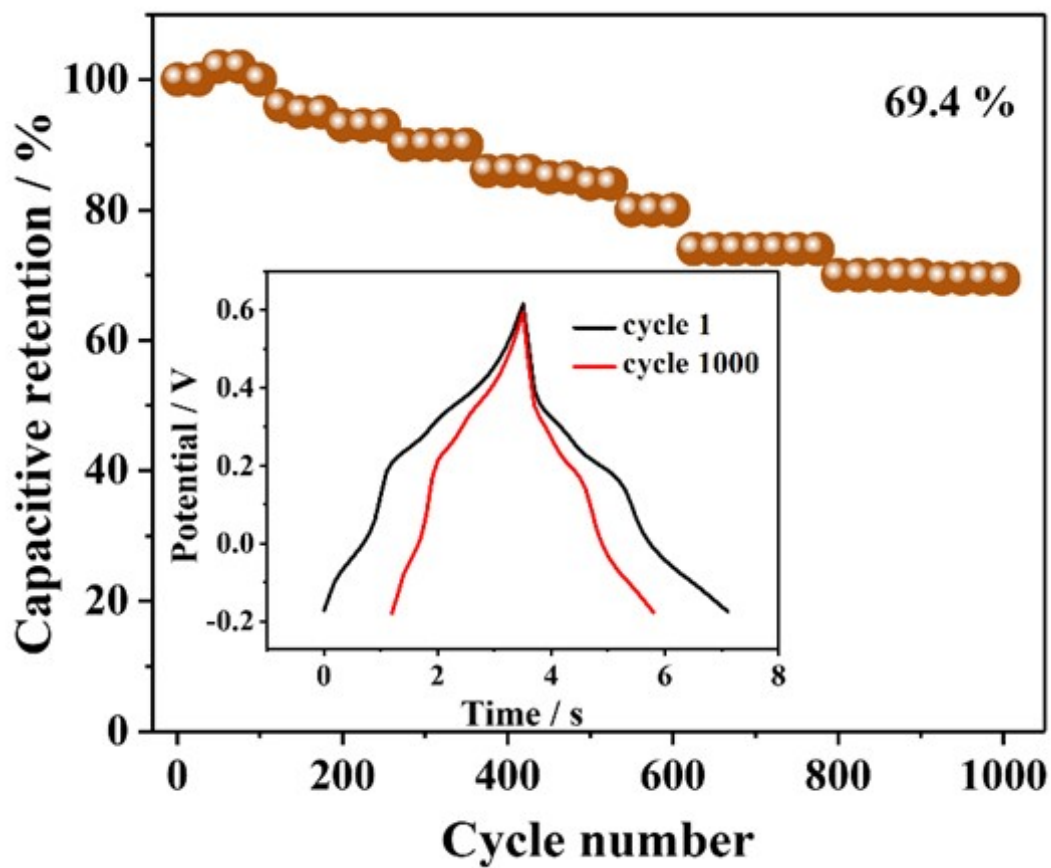


Fig. S15. The capacitance retention rate of  $\text{PMo}_{12}\text{-GCE}$  after 1000 charge-discharge cycles at a current density of  $10 \text{ A g}^{-1}$  (zoomed GCD curves before and after the stability test)

V. FT-IR of 1 immersed in a mixed solution of 0.5 M H<sub>2</sub>SO<sub>4</sub> + 0.5 M Na<sub>2</sub>SO<sub>4</sub> (v:v = 1:1) for 6, 12, 24, 48, and 96 h

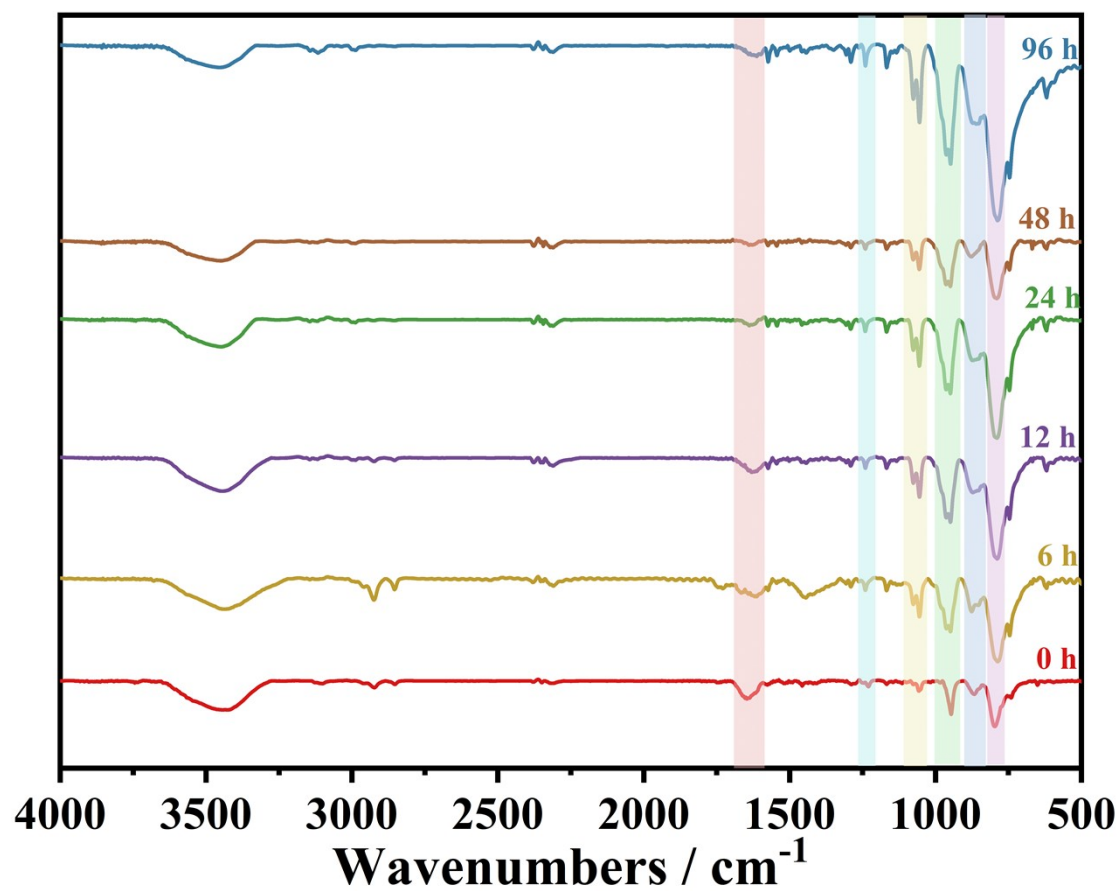


Fig. S16. The FT-IR of 1 immersed in 0.5 M H<sub>2</sub>SO<sub>4</sub> + 0.5 M Na<sub>2</sub>SO<sub>4</sub> for 0, 6, 12, 24, 48 and 96 h

VI. FT-IR of 2 immersed in a mixed solution of 0.5 M H<sub>2</sub>SO<sub>4</sub> + 0.5 M Na<sub>2</sub>SO<sub>4</sub> (v:v = 1:1) for 6, 12, 24, 48, and 96 h

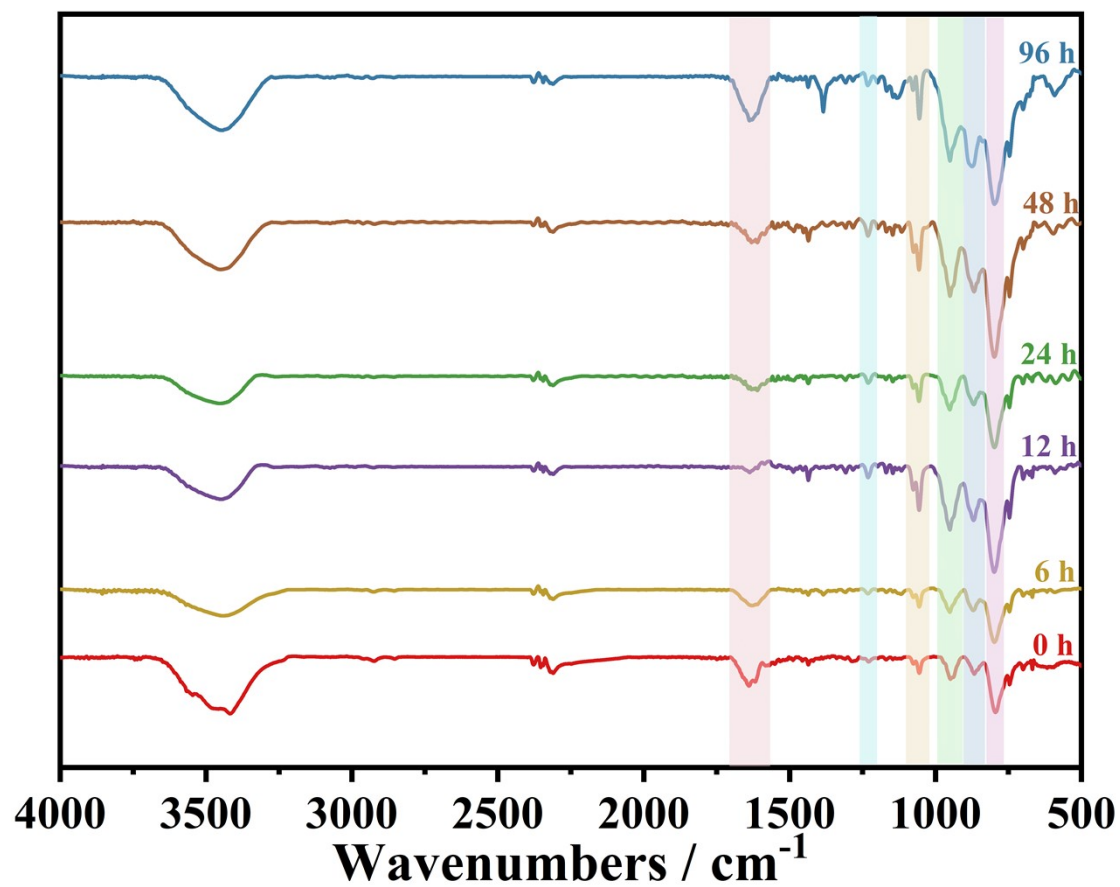


Fig. S17. The FT-IR of 2 immersed in 0.5 M H<sub>2</sub>SO<sub>4</sub> + 0.5 M Na<sub>2</sub>SO<sub>4</sub> for 0, 6, 12, 24, 48 and 96 h

VII. XRD of 1 and 2 immersed in a mixed solution of 0.5 M H<sub>2</sub>SO<sub>4</sub> + 0.5 M Na<sub>2</sub>SO<sub>4</sub>  
(v:v = 1:1) for 6, 12, 24, 48, and 96 h

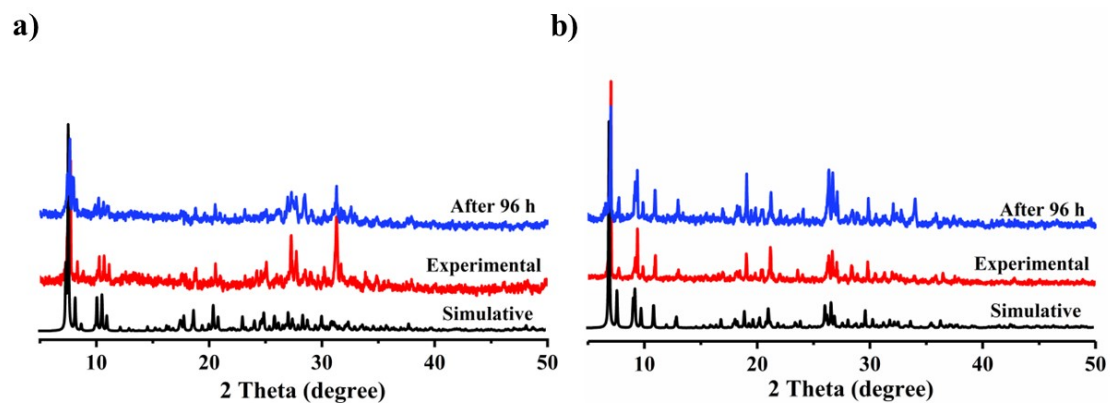


Fig. S18. The XRD of a)1 and b) 2 immersed in 0.5 M H<sub>2</sub>SO<sub>4</sub> + 0.5 M Na<sub>2</sub>SO<sub>4</sub> for 0, 6, 12, 24, 48 and 96 h

### Section 3 References

1. Liu, Q. Q.; Wang, X. L.; Lin, H. Y.; Chang, Z. H.; Zhang, Y. C.; Tian, Y.; Lu, J. J.; Yu, L., Two new polyoxometalate-based metal–organic complexes for the detection of trace Cr(vi) and their capacitor performance. *Dalton Trans.* **2021**, 50 (27), 9450-9456.
2. Wang, J.; Huang, M.; Liu, P.; Cheng, W., Synthesis and characterization of two infinite coordination networks from flexible unsymmetric ligands. *J. Mol. Struct.* **2008**, 875 (1-3), 22-26.
3. Xu, X.; Zhang, J.; Zhang, Z.; Lu, G.; Cao, W.; Wang, N.; Xia, Y.; Feng, Q.; Qiao, S., All-Covalent Organic Framework Nanofilms Assembled Lithium-Ion Capacitor to Solve the Imbalanced Charge Storage Kinetics. *Nano-Micro Lett.* **2024**, 16 (1), 116.
4. Tang, K.; Yu, X.; Sun, J.; Li, H.; Huang, X., Kinetic analysis on LiFePO<sub>4</sub> thin films by CV, GITT, and EIS. *Electrochim. Acta*, **2011**, 56 (13): 4869-4875.
5. Liu, Y.; Liu, S.; He, D.; Li, N.; Ji, Y.; Zheng, Z.; Luo, F.; Liu, S.; Shi, Z.; Hu, C., Crystal facets make a profound difference in polyoxometalate-containing metal–organic frameworks as catalysts for biodiesel production. *J. Am. Chem. Soc.*, **2015**, 137 (39): 12697-12703.